

AN IMPROVED METHOD FOR COMPUTING A DISCRETE HANKEL TRANSFORM

H. FISK JOHNSON

Department of Applied and Engineering Physics, Cornell University, 212 Clark Hall, Ithaca, NY 14853, USA

Received 5 June 1986

A new and simple algorithm for computing a discrete Hankel transform, which does not rely on the fast Fourier transform is described. In the solution of certain types of differential equations this algorithm can provide a major improvement in speed and accuracy over previously described methods. An application to a particular form of the transport equation relevant to a class of problems in electron scattering is given.

1. Introduction

The Hankel transform has proven to be extremely useful in problems associated with optics, geophysics, electron scattering and many other areas. Recently, many methods have been proposed for computing a discrete form of this transform [1–8]. Most of these methods have been described in the literature as “quasi-fast” since they take advantage of the speed of the fast Fourier transform algorithm. In this paper we report on a new algorithm which is finite, and which does not rely on the fast Fourier transform.

The algorithm which we describe provides a number of advantages over previously described methods. First, the algorithm is simple and easy to implement. Secondly, this algorithm has the same reciprocity properties of the continuous transform, and it is hoped that further study of the unique symmetry properties of this discrete transform will lead to a truly fast algorithm in which a fast Fourier transform is not utilized. Lastly, this algorithm can provide a moderate improvement in speed and accuracy over most other algorithms for the straight-forward computation of a Hankel transform, and provide a major improvement in speed and accuracy in problems in which a “back” transform of related nature is needed, such as in a convolution, or the solution of various types of differential equations. An application to a problem of such a nature, namely the solution of a particular form of the transport equation relevant to a class of problems in electron scattering, will be given.

2. Hankel transform – a definition and review

We can write Hankel’s generalization of the Fourier–Bessel transform of $f(x)$ as

$$F_\nu(R) = \int_0^\infty f(x) J_\nu(xR) x \, dx, \quad \nu \geq -1/2, \quad (1)$$

where the reverse transform is given by

$$f(x) = \int_0^\infty F_\nu(R) J_\nu(xR) R \, dR, \quad \nu \geq -1/2, \quad (2)$$

where

$$\int_0^\infty f(x) x^{1/2} \, dx \quad (3)$$

must exist and be absolutely convergent, and where $f(x)$ satisfies Dirichlet's conditions (of limited total fluctuation) in the interval $[0, \infty]$.

For the purpose of determining a discrete transform we will assume that $f(x) = 0$ for all $x > T$, and define $r = RT/j_N$ ($j_N = N$ th zero of $J_\nu(x)$) so that the forward transform can be written as

$$F_\nu(rj_N/T) = T^2 \int_0^1 f(xT) J_\nu(xrj_N) x \, dx \quad (4)$$

and the reverse transform is written as

$$f(xT) = \frac{j_N^2}{T^2} \int_0^\infty F_\nu(rj_N/T) J_\nu(xrj_N) r \, dr. \quad (5)$$

We can now expand $f(xT)$ over $[0, 1]$ using Lommel's generalized version of the Fourier-Bessel series [9], namely,

$$f(xT) = \begin{cases} \sum_{m=1}^{\infty} \frac{2C_m}{J_{\nu+1}^2(j_m)} J_\nu(j_m x), & 0 \leq x \leq 1, \\ 0, & 1 < x \leq \infty, \end{cases} \quad (6)$$

where j_m are the zeros of $J_\nu(x)$ arranged in ascending order, and where the coefficients C_m are given by

$$C_m = \int_0^1 x f(xT) J_\nu(j_m x) \, dx. \quad (7)$$

We now make the additional assumption that $C_m = 0$ for all $m \geq N$. Since we can choose N and T arbitrarily large, we suffer no loss of generality by having imposed this additional assumption on the properties of $f(xT)$. Taking the transform of eq. (6) utilizing eq. (4), we obtain the well established result that

$$F_\nu(j_m/T) = T^2 C_m \quad \text{when} \quad r = j_m/j_N \quad (8)$$

and

$$F_\nu(rj_N/T) = \sum_{m=1}^{N-1} \frac{2F_\nu(j_m/T) J_\nu(rj_N) j_m}{J_{\nu+1}^2(j_m) (j_m^2 - r^2 j_N^2)}, \quad 0 \leq r \leq \infty. \quad (9)$$

Applying eq. (8) to eq. (6) we also see that

$$f(xT) = \begin{cases} \sum_{m=1}^{N-1} \frac{2F_\nu(j_m/T)}{J_{\nu+1}^2(j_m) T^2} J_\nu(j_m x), & 0 \leq x \leq 1, \\ 0, & 1 < x \leq \infty. \end{cases} \quad (10)$$

3. A new discrete Hankel transform algorithm

This last equation gives an exact relationship between $f(xT)$ and the values of its transform at particular values of r . We now need a similar relationship, relating $F_\nu(rj_N/T)$ to values of $f(xT)$ at particular values of x . In order to derive this relationship we make use of the following orthogonality relation (the derivation of which is in appendix A).

$$\frac{4}{J_{\nu+1}^2(j_m) j_N^2} \sum_{p=1}^{N-1} \frac{J_\nu(j_m j_p/j_N) J_\nu(j_i j_p/j_N)}{J_{\nu+1}^2(j_p)} = \delta_{m,i}, \quad m, i < N. \quad (11)$$

Setting $x = j_p/j_N$ in eq. (10), multiplying both sides by $J_\nu(j_p j_i/j_N)$, and summing, one obtains

$$F_\nu(j_i/T) = \frac{T^2}{j_N^2} \sum_{p=1}^{N-1} \frac{2J_\nu(j_p j_i/j_N)}{J_{\nu+1}^2(j_p)} f(j_p T/j_N). \quad (12)$$

Therefore, we can write an exact pair of discrete transform equations as

$$f(i) = \frac{1}{T^2} \sum_{m=1}^{N-1} Y_\nu(m, i) F_\nu(m), \quad F_\nu(m) = \frac{T^2}{j_N^2} \sum_{i=1}^{N-1} Y_\nu(m, i) f(i), \quad (13)$$

where

$$F_\nu(m) = F_\nu(j_m/T), \quad f(i) = f(j_i T/j_N), \quad Y_\nu(i, m) = 2J_\nu(j_i j_m/j_N)/J_{\nu+1}^2(j_m).$$

This now can be taken a step further. If we insert eq. (12) into eq. (9) we obtain a relationship between $f(p)$ and $F_\nu(rj_N/T)$ at continuous values of r .

$$F_\nu(rj_N/T) = \frac{T^2}{j_N^2} \sum_{p=1}^{N-1} \frac{2f(j_p T/j_N)}{J_{\nu+1}^2(j_p)} \sum_{m=1}^{N-1} \frac{2J_\nu(j_m j_p/j_N) J_\nu(rj_N) j_m}{J_{\nu+1}(j_m)(j_m^2 - r^2 j_N^2)}.$$

This can be further simplified by recognizing that the inner sum on the right-hand side of the above equation is the first $N-1$ terms in the Fourier-Bessel series for $J_\nu(j_p r)$. We can therefore write for $r < 1$

$$F_\nu(rj_N/T) \approx \frac{T^2}{j_N^2} \sum_{p=1}^{N-1} \frac{2f(j_p T/j_N)}{J_{\nu+1}^2(j_p)} J_\nu(j_p r) + \epsilon, \quad (14)$$

where

$$\epsilon = \frac{T^2}{j_N^2} \sum_{p=1}^{N-1} \frac{2f(j_p T/j_N)}{J_{\nu+1}^2(j_p)} \sum_{m=N}^{\infty} \frac{2J_\nu(j_m j_p/j_N) J_\nu(rj_N) j_m}{J_{\nu+1}(j_m)(j_m^2 - r^2 j_N^2)}. \quad (15)$$

For most functions $f(xT)$, the error in approximation (14) rapidly becomes small for increasing values of N . In fact, for values of N greater than 10 this error can be less than 1%. An example will be given in the next section.

By further utilizing the methods used in appendix A, additional orthogonality relations can be derived. Some of these relations include the following (see appendices B and C for proofs and additional relations),

$$\sum_{m=1}^{N-1} \frac{2J_\nu(\lambda_m j_r/j_N) J_\nu(\lambda_m j_p/j_N)}{J_\nu^2(\lambda_m) j_N^2} = \delta_{p,r} \frac{J_{\nu+1}^2(j_p)}{2} - \frac{2(\nu+1) J_r^\nu j_p^\nu}{J_N^{2(\nu+1)}} + \epsilon_1(N), \quad (16)$$

$\lambda_m \equiv m$ th zero of $J_{\nu+1}(x)$,

$$\sum_{m=1}^N \frac{2J_{\nu+1}(j_m \lambda_k/\lambda_N) J_{\nu+1}(j_m \lambda_p/\lambda_N)}{J_{\nu+1}^2(j_m) \lambda_N^2} = \delta_{p,k} \frac{J_\nu^2(\lambda_p)}{2} + \epsilon_2(N), \quad (17)$$

$$\sum_{m=1}^{N-1} \frac{2J_{\nu+1}(\lambda_m j_p/\lambda_N) J_{\nu+1}(\lambda_m j_r/\lambda_N)}{J_\nu^2(\lambda_p) \lambda_N^2} = \delta_{p,r} \frac{J_{\nu+1}^2(j_r)}{2} - \frac{J_{\nu+1}(j_r) J_{\nu+1}(j_p)}{2N} + \epsilon_3(N), \quad (18)$$

$$\sum_{m=1}^{N-1} \frac{2j_N}{j_m} \frac{J_{\nu+1}(\lambda_k j_m/j_N) J_\nu(j_m j_p/j_N)}{J_{\nu+1}^2(j_m) j_N^2} = \int_0^1 J_\nu(x j_p) J_{\nu+1}(x \lambda_k) dx + \epsilon_4(N), \quad (19)$$

where numerical analysis indicates that for $\nu = 0$

$$\begin{aligned}\epsilon_1(N) &< 0.014 j_k j_p / j_N^3, & k, p < N, & N > 3, \\ \epsilon_2(N) &< 0.012 j_k j_p / j_N^3, & k, p < N, & N > 3, \\ \epsilon_3(N) &< 0.024 j_N^{1.5}, & k, p < N, & N > 3, \\ \epsilon_4(N) &< 0.015 (j_k j_p)^{1.5} / j_N^3, & k, p < N, & N > 3.\end{aligned}$$

These additional relations combined with the original orthogonality relation in eq. (11) may prove to be useful in numerically computing the solutions to various types of differential equations which require Hankel transforms.

4. Examples – speed and accuracy

It is first illustrative to make a direct comparison of a typical FFT method for computing a Hankel transform to the method described above. The method chosen for comparison, is that of Candel [2] which calculates the HT by means of a single one dimensional FFT followed by repeated summations of pre-selected Fourier components. This method involves $M \log_2 M$ multiplications and $M^2 + M \log_2 M$ additions whereas our method requires N^2 multiplications and additions. As shall be seen, we can choose N to be considerably smaller than M not only because of the faster convergence rate of our method, but also because there is no need to double the size of the array by extending it from $[0, \infty]$ to the interval $[-\infty, \infty]$ for purposes of computing the FFT.

The first two examples we choose are those presented by Candel [2], the discontinuous function

$$f_1(\xi) = \begin{cases} 1, & \xi < a, \\ 0, & \xi > a \end{cases}$$

which has the analytic transform

$$F(r) = aJ_1(ar)/r$$

and the reciprocal of the above, namely

$$f_2(\xi) = aJ_1(a\xi)/\xi$$

which has the transform

$$F(r) = \begin{cases} 1, & r \leq a, \\ 0, & r > a. \end{cases}$$

For the purpose of separating $f_1(\xi)$ and $f_2(\xi)$ into discrete points we choose

$$f_1(n) = \begin{cases} 1, & |n| \leq h, \\ 0, & |n| > h, \end{cases}$$

where

$$n = 1, \dots, N, \quad T = \pi N/2 \quad \text{for our transform,}$$

$$n = -M/2, -M/2 + 1, \dots, M/2 - 1, M/2, \quad T' = \pi M \quad \text{for Candel's transform}$$

and

$$f_2(n) = J_1(j_n T / j_N) / (j_n T / j_N), \quad n = 1, \dots, N, \quad T = \pi N/4$$

for our transform, and

$$f_2(n) = \begin{cases} J_1(2nT'/M)/(2nT'/M), & n = 1, \dots, M/2, \\ 1/2, & n = 0, \\ J_1(2(n-1)T'/M)/(2(n-1)T'/M), & n = -1, \dots, -M/2 \end{cases}$$

for Candel's transform.

As a last example we choose $f_3(\xi) = (\xi^2 + 1)^{-2}$ which has applications in problems dealing with the elastic scattering of electrons. In this case, the analytic transform is $F(r) = rK_1(r)/2$, where $K_1(r)$ is the first order modified Hankel function.

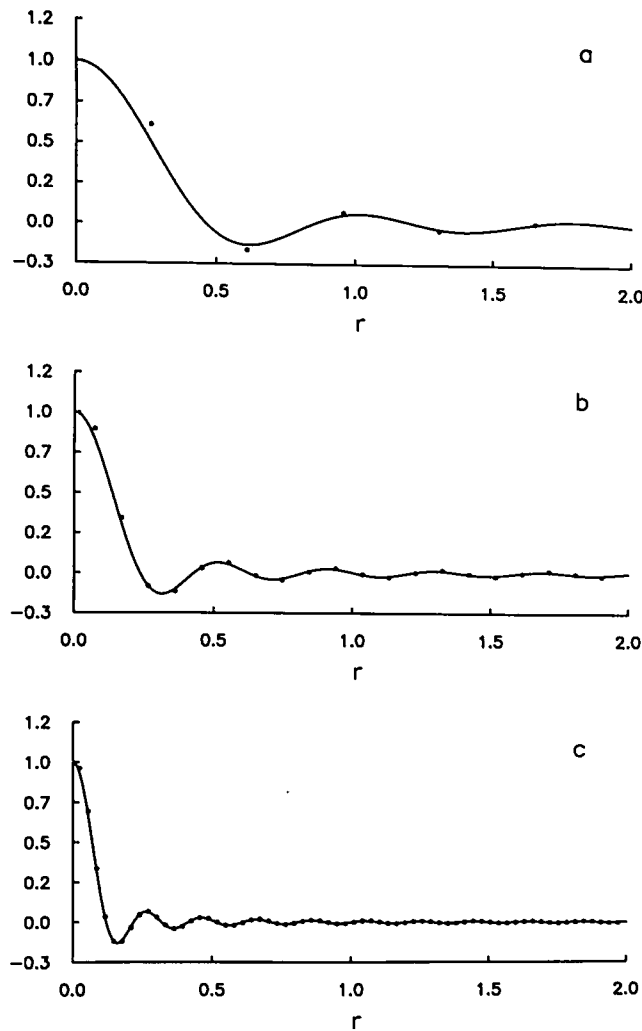


Fig. 1. Transform of the step function $f_1(\xi)$ using our method. The solid line is the exact transform, the dots are the numerical transform. (a) $N = 5, h = 5$; (b) $N = 20, h = 10$; (c) $N = 64, h = 20$.

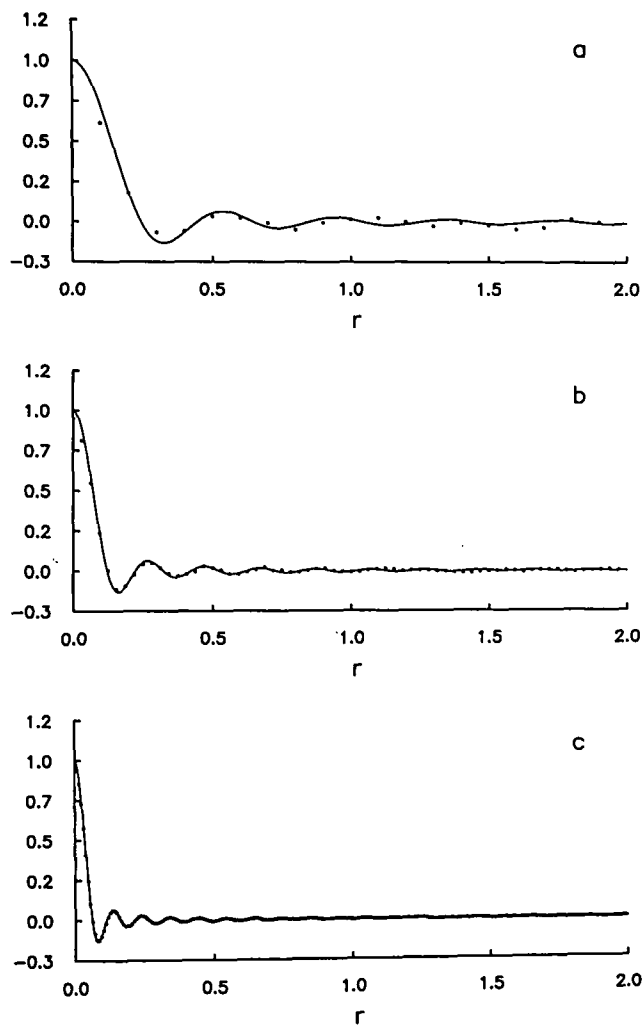


Fig. 2. Transform of the step function $f_1(\xi)$ using Candel's method. The solid line is the exact transform, the dots are numerical transform. (a) $M = 40$, $h = 10$; (b) $M = 128$, $h = 20$; (c) $M = 512$, $h = 40$.

The results for these three examples are given in figs. 1–6. In all cases, the free parameters h , T , T' were chosen so that a rough attempt was made to optimize the accuracy of the transform for the given value of N or M .

As can be seen from these figures, our method represents a considerable improvement in accuracy for similar values of the total number of discrete points utilized in the transform. We also notice from the error between the discrete transform and the actual transform that Candel's method of computing the HT introduces an additional quantity of "noise" into the final result, a consequence of the approximate integration rules utilized in summing pre-selected Fourier components in this method of the HT.

We can now make a closer examination of the approximation in eq. (14). Fig. 7 and 8 show a comparison of eqs. (14) and (9) for the first two examples. In all cases, it can be seen that eq. (9) converges rapidly to eq. (14) and that for $N > 10$ there exists very little difference in these plots.

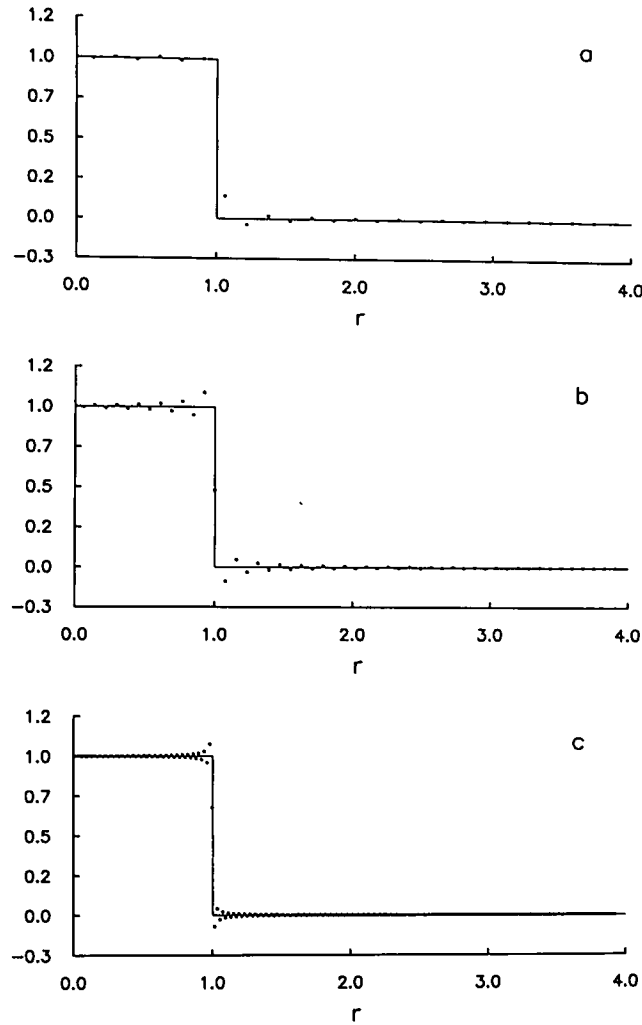


Fig. 3. Transform of $f_2(\xi) = \alpha J_1(\alpha \xi) / \xi$ using our method. The solid line is the exact transform, the dots are the numerical transform. (a) $N = 25$, $T = 20$; (b) $N = 50$, $T = 40$; (c) $N = 200$, $T = 160$.

It is now necessary to consider the speed of our transform. As previously noted, Candel's algorithm requires approximately $M \log_2 M$ multiplications and M^2 additions, whereas our algorithm requires N^2 multiplications and additions. As evidenced in figs. 1–8, N can be chosen to be considerably smaller than M in order to achieve the same degree of accuracy. An earlier paper by Brunol and Chavel [1], which compares an algorithm similar to ours to a typical FFT method of computing the HT indicates that the Brunol and Chavel method of computing the HT is marginally quicker than a typical FFT algorithm for computing a HT to the same degree of accuracy. Both the Brunol and Chavel method and our method rely on the convergence of a Fourier–Bessel expansion in the computation of the HT. One would expect therefore, that our algorithm would be similar in speed and accuracy.

The real advantage in speed for our algorithm does not, however, manifest itself directly in examples where a straight-forward HT is performed on a representative function. Rather, the speed advantage of our

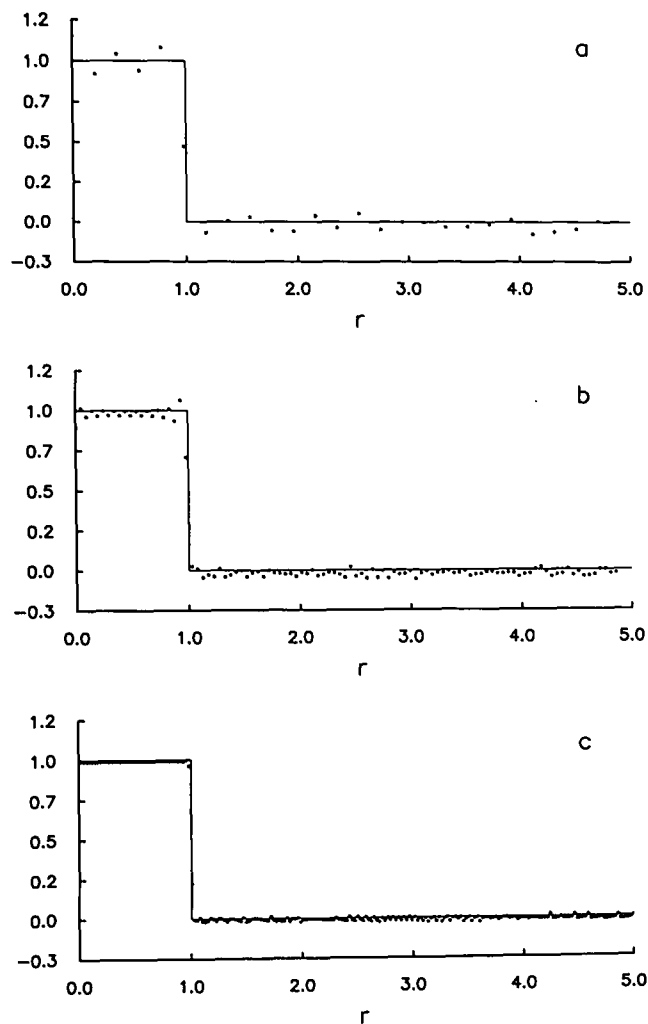


Fig. 4. Transform of $f_2(\xi) = aJ_1(a\xi)/\xi$ using Candel's method. The solid line is the exact transform, the dots are the numerical transform. (a) $M = 50$, $T = 16$; (b) $M = 200$, $T = 64$; (c) $M = 512$, $T = 128$.

algorithm is seen most clearly in applications to the solution of various differential equations where it is necessary to follow a forward HT with a 'reverse' or related type of transform. In these examples our method can represent an order of magnitude or more improvement in speed. An example is given in the next section.

5. Successive forward-backward transforms

One particular application in electron microscopy in which the advantage of our algorithm is demonstrated is that of the case of computing the intensity of collected electrons which have undergone plural scattering in traversing a specimen of thickness t and are then collected through an aperture of semi-angle α .

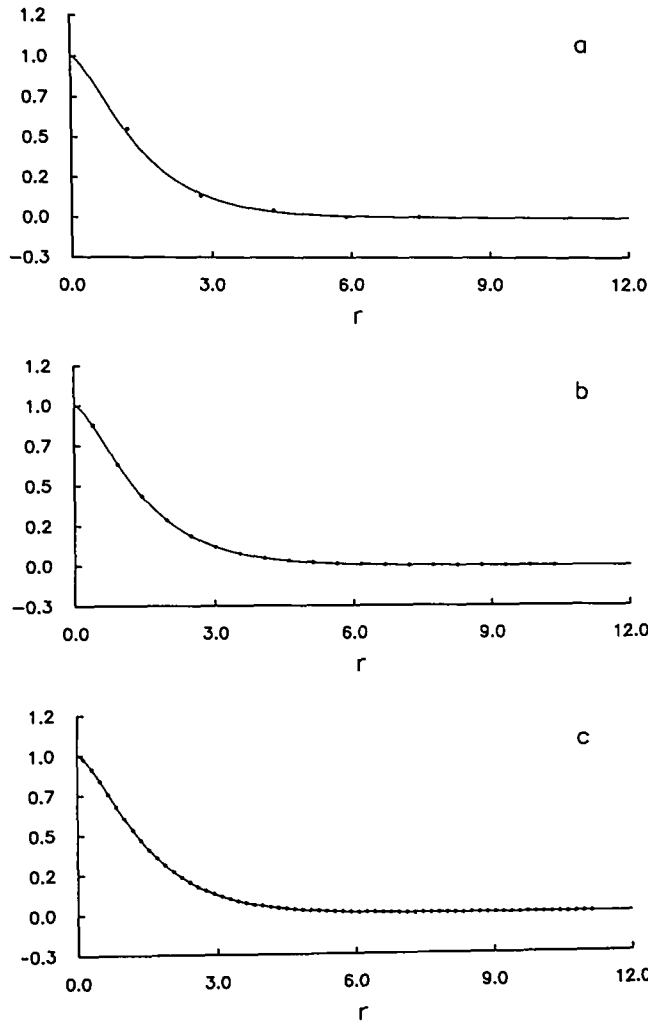


Fig. 5. Transform of $f_3(\xi) = 1/(\xi^2 + 1)^2$ using our method. The solid line is the exact transform, the dots are the numerical transform. (a) $N = 5, T = 2.0$; (b) $N = 20, T = 6.0$; (c) $N = 64, T = 18$.

The angular distribution of an electron beam which has undergone plural scattering can be derived as a solution to a particular form of the transport equation [10], namely

$$\frac{\partial I(t, |\mathbf{q}|)}{\partial t} = -\frac{1}{\lambda} I(t, |\mathbf{q}|) + \frac{1}{\lambda} \int_{-\pi}^{+\pi} d\phi \int_0^{\infty} I(t, |\boldsymbol{\theta}|) p(|\mathbf{q} - \boldsymbol{\theta}|) \theta d\theta, \quad (20)$$

where

$$|\mathbf{q} - \boldsymbol{\theta}|^2 = q^2 + \theta^2 - 2q\theta \cos \phi,$$

\mathbf{q} = momentum transfer vector, $p(|\mathbf{q}|)$ is the axially symmetric single scattering probability distribution normalized to unit intensity, i.e. $\int p(|\mathbf{q}|) d\Omega = 1$, $I(t, |\mathbf{q}|)$ = multiply scattered beam intensity, λ = mean free path for single scattering.

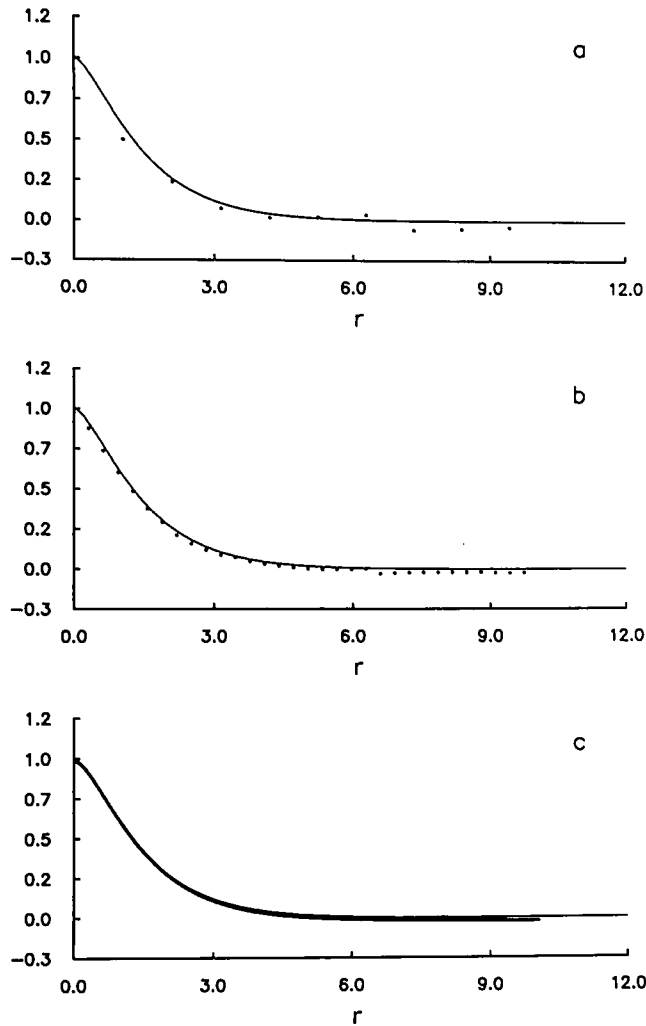


Fig. 6. Transform of $f_3(\xi) = 1/(\xi^2 + 1)^2$ using Candel's method. The solid line is the exact transform, the dots are the numerical transform. (a) $M = 20$, $T = 3.0$; (b) $M = 64$, $T = 10.0$; (c) $M = 512$, $T = 80$.

This differential equation can be solved by taking the Hankel transform of both sides, slightly rearranging terms and integrating. After subtracting the unscattered beam (in order to avoid numerical difficulties) one obtains

$$\hat{I}(t, \hat{q}) = I_0 e^{-t/\lambda} [e^{t\beta(\hat{q})/\lambda} - 1],$$

where $\hat{\cdot}$ denotes the transformed variables and function, and I_0 denotes the incident beam intensity. The "collected" beam intensity can then be written

$$\int_0^\alpha I(t, q) q dq = \int_0^\alpha q dq \int_0^\infty I_0 e^{-t/\lambda} [e^{t\beta(\hat{q})/\lambda} - 1] J_0(q\hat{q}) \hat{q} d\hat{q}. \quad (21)$$

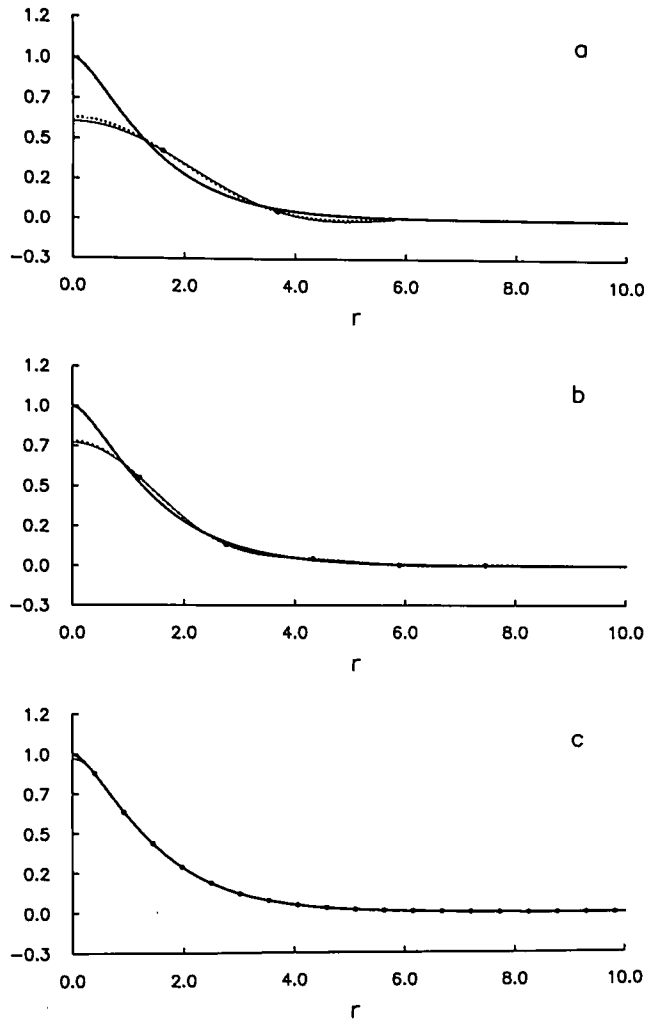


Fig. 7. A comparison of eqs. (9) and (14) for the transform of the function $f_3(\xi) = 1/(\xi^2 + 1)^2$. The thick solid line is the exact transform, the thin solid line is a plot of eq. (14), and the dotted line is a plot of eq. (9). (a) $N = 2$, $T = 1.5$; (b) $N = 5$, $T = 2.0$; (c) $N = 20$, $T = 2.0$.

After reversing the order of integration we obtain

$$\int_0^\alpha I(t, q) q \, dq = \alpha I_0 e^{-t/\lambda} \int_0^\infty [e^{t\hat{p}(\hat{q})/\lambda} - 1] J_1(\hat{q}\alpha) \, d\hat{q}. \tag{22}$$

Ordinarily one may numerically compute this result in any one of a number of ways. Once the transform of $p(q)$ is computed, one can either take the back transform of $I_0 e^{-t/\lambda} [e^{t\hat{p}(\hat{q})/\lambda} - 1]$ and numerically integrate such as in eq. (21), or one can numerically integrate eq. (22) directly. Both of these procedures are extraordinarily inefficient. In the first case, one needs to compute *two* full $N \times N$ transforms in addition to a numerical integration in order to obtain the result for a single value of α . In the second case, the numerical integration of eq. (21) directly, requires a large number of steps, particularly for larger values of α , because of the degree of fluctuation of the function $J_1(q\alpha)$ [4]. Most importantly, it should be noted

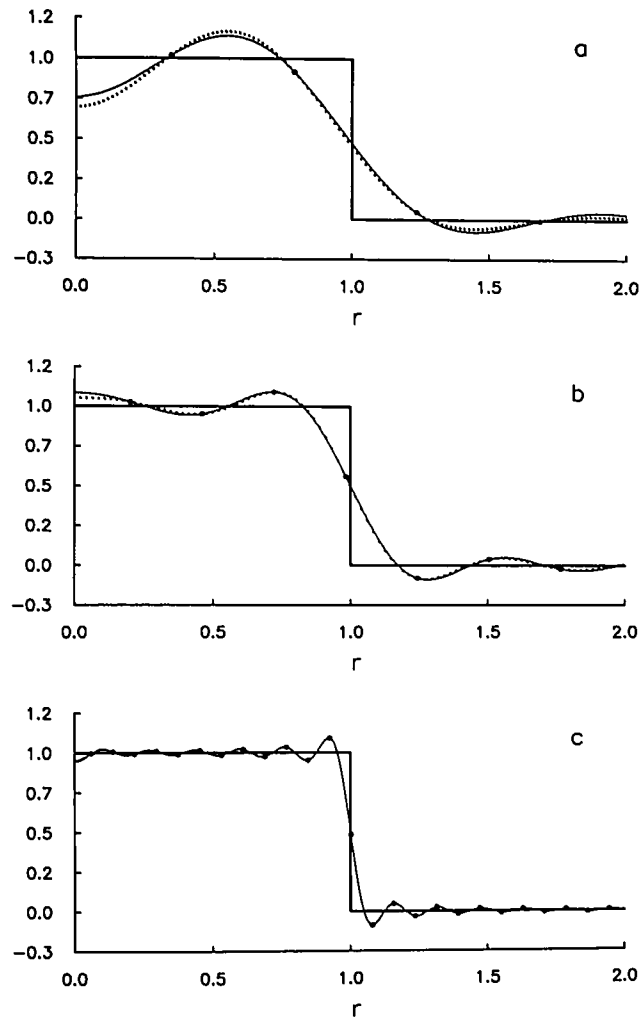


Fig. 8. A comparison of eqs. (9) and (14) for the transform of the function $f_2(\xi) = aJ_1(a\xi)/\xi$. The thick solid line is the exact transform, the thin solid line is a plot of eq. (14), and the dotted line is a plot of eq. (9). (a) $N = 4$, $T = 7$; (b) $N = 10$, $T = 12$; (c) $N = 50$, $T = 40$.

that one cannot simply evaluate eq. (22) by attempting a back HT of order 1 because the transforming function does *not* satisfy the convergence criteria of eq. (3).

All these inefficiencies can be overcome by utilizing eqs. (13) and a variation of eq. (19), results which take advantage of the basic underlying properties of Bessel functions. To do this, we first compute values of $\hat{p}(j_i/T)$ using algorithm (13). We then can compute the value of the function

$$\hat{G}(j_i/T) = I_0 e^{-t/\lambda} (e^{t\hat{p}(j_i/T)/\lambda} - 1). \quad (23)$$

This first step is a procedure which is similar to any other method for solving this problem, except that the algorithm in eq. (23) generates the coefficient $\hat{G}(j_i/T)$ free of the “noise” that results from approximate integration rules used in typical FFT algorithms.

In order to take the “back” transform as indicated by eq. (22), we first notice that eq. (9) can be analytically integrated using a variation on Hankel’s integral [11] (see appendix C) to obtain the exact result

$$\int_0^\infty F_0(rj_N/T)J_1(rxj_N) dr = \sum_{k=1}^N \frac{2F_0(j_k/T)J_1(j_kx)}{j_Nj_kJ_1^2(j_k)}. \tag{24}$$

This relationship can then be combined with eq. (22) to obtain the solution

$$\int_0^\alpha I(t, q)q dq = \alpha \sum_{k=1}^N \frac{2\hat{G}(j_k/T)J_1(j_k\alpha/T)}{j_kJ_1^2(j_k)T}. \tag{25}$$

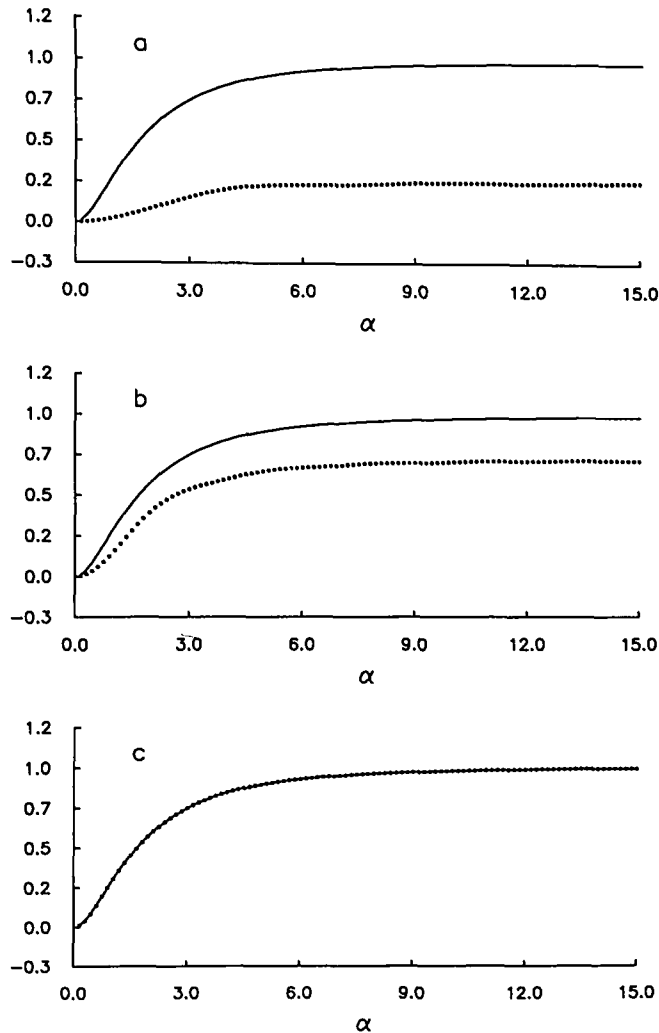


Fig. 9. A demonstration of the rate of convergence of eq. (25) in calculating the intensity of collected electrons which have undergone plural scattering in traversing a specimen of thickness $t = 2\lambda$. The elastic scattering differential cross section utilized is that given by eq. (26) for $\theta_0 = 1$, $I_0 = 1$. The solid line represents the exact value of $\int_0^\alpha I(t, q)q dq$ and the dotted line represents the computed numerical value. (a) $N = 5$, $T = 15$; (b) $N = 10$, $T = 15$; (c) $N = 30$, $T = 15$.

Thus the final step of this calculation for a particular value of α , has been reduced to a simple N step summation, which is noise free.

To illustrate this we can take a simple model for the probability of elastic scattering of electrons through a solid state medium such as [12]

$$p(\theta) = \frac{1}{(\theta^2 + \theta_0^2)^2} \frac{1}{4\theta_0^2}, \quad (26)$$

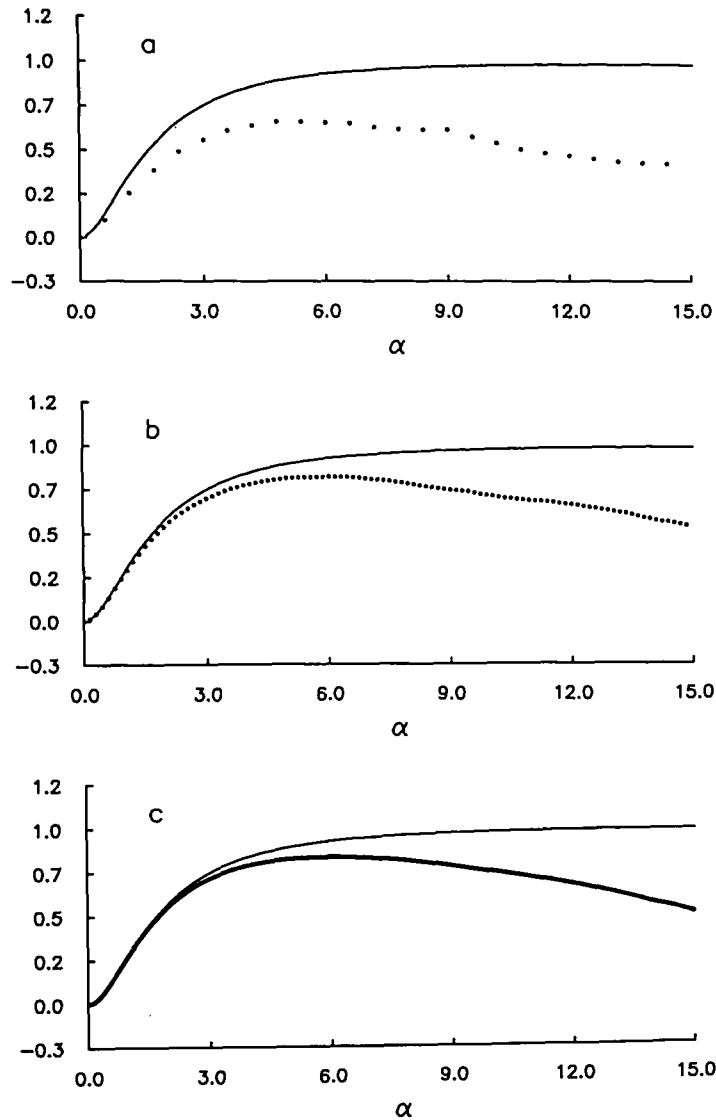


Fig. 10. A demonstration of the rate of convergence of the application of Candel's method of the HT in computing the intensity of collected electrons which have undergone plural scattering in traversing a specimen of thickness $t = 2\lambda$. The elastic scattering differential cross section utilized is that given by eq. (26) for $\theta_0 = 1$, $I_0 = 1$. The solid line represents the exact value of $\int_0^\alpha I(t, q) q \, dq$ and the dotted line represents the computed numerical value. (a) $M = 50$, $T = 15$; (b) $M = 200$, $T = 15$; (c) $M = 1000$, $T = 15$.

where θ_0 is some characteristic scattering angle and $p(\theta)$ is the normalized differential cross section for the elastic scattering of an electron through an angle θ .

It is illustrative to first generate the curve for the intensity of collected electrons, scattered through a specimen of thickness $t = 2\lambda$ as a function of collection aperture halfangle α . From fig. 9, it can be seen that eq. (25) rapidly converges to the exact result. In this figure the dotted line represents eq. (25) for various values of N and the solid lines represents the exact result computed for the limiting case $N \gg 100$ for eq. (25). It can be seen for values of $N = 30$ the computed result is indistinguishable from the real result.

On the other hand, if one generates this curve by taking the forward and back HT utilizing Candel's method and then numerically integrating (as in eq. (21)) one obtains the result in fig. 10. As can be seen, this method totally fails for large angles α . The reason for this result is that simply summing "pre-selected Fourier components", leads to integration errors which are compounded when one back transforms and then numerically integrates. This problem can of course be overcome by utilizing more exact integration methods in summing Fourier components (as discussed in Candel's paper), but of course this leads to much longer computation times. Whereas, the curve in the bottom of fig. 9 is generated via two transforms utilizing $N' \times N'$ operation ($N' = 30$), FFT methods require at least two transforms requiring $M \log_2 M$ operations followed by an M step numerical integration (where $M > 200$ and where great care must be taken in choosing approximate integration methods). Clearly this is a more complicated procedure.

In a typical contrast calculation of importance to electron microscopy, such as those made by Crewe and Groves [13], one is ultimately interested in computing the intensity of collected electrons as a function of specimen thickness. Our method of making this calculation is particularly suited to generating this curve. As indicated by eq. (25), after the array $\hat{p}(j_i/T)$ is generated, one simply needs to compute the values of $\hat{G}(\hat{q})$ followed by an N step summation for each value of α . On the other hand, utilizing eq. (21) and a typical FFT method for computing the HT, one would need to perform a full $M \log_2 M$ transform followed by a numerical integration for each value of α . Generating L points in the curve requires in the first case, $N \times L$ "operations" (where $N \approx 30$) whereas the second case requires on the order of

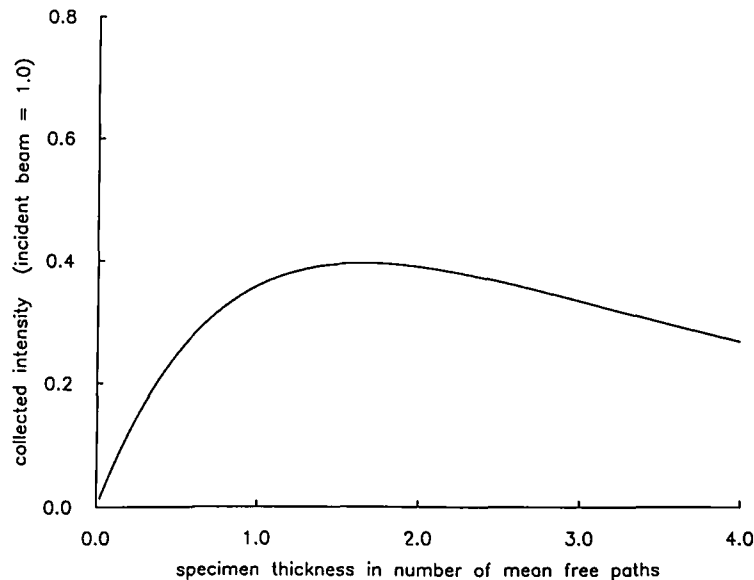


Fig. 11. A computation of $\int_0^\alpha I(t, q) q \, dq$ as a function of specimen thickness utilizing eq. (25).

$(M \log M + M) \times L$ “operations” (where $M > 200$). Thus in general, these methods differ in computation time by a factor of about L . In a typical application $L \approx 100$ so computation times may be as much as 100 times faster. Of course, it may be more efficient to numerically integrate eq. (22) directly, but because of the degree of fluctuation on the function $J_1(q\alpha)$ the numerical integration will still require a very large number of steps, and thus utilizing eq. (24) remains considerably more efficient.

Fig. 11, illustrates the use of eq. (24), to generate the required curve. In this example $N = 50$, $\theta = 1.0$, $\alpha = 1.5$ and $I_0 = 1.0$. This curve took less than a few seconds to generate on a Prime 750 computer utilizing the Primos 19.4.2 operating system.

5. Discussion

We have seen that utilizing the algorithm in eq. (13) for the purpose of computing a numerical HT can afford a number of advantages over those algorithms previously discussed in the literature. As evidenced by the work of Brunol and Chavel [1], algorithms which rely on the convergence of a standard Fourier–Bessel series expansion, such as that of eq. (13), take less computation time to achieve the same degree of accuracy as standard FFT methods for computing a straight-forward Hankel transform. Additionally, in some applications, particularly those in which a follow up back transform is needed, the use of our algorithm can lead to a considerable reduction in computation time. The reason for this dramatic improvement is two fold. First, errors introduced through approximate integration rules, a characteristic of standard FFT methods of computing the HT, are not compounded when making a follow up transform. Secondly, in some applications it may be necessary and possible to analytically integrate eq. (9) or eq. (14), as in the last example. It may additionally be possible to use one of the relationships in eqs. (16)–(19) in determining a solution. For example, eq. (15) may be relevant to problems in which Dini’s expansion [11] is required.

In summary, in solving a differential equation requiring Hankel transforms, one may be able to dramatically improve the speed of calculation utilizing some of the fundamental principles outlined in this paper. It is also hoped that further study of some of the unique symmetries of our particular algorithm may lead to the development of a truly fast algorithm.

Acknowledgements

The author is indebted to Prof. Michael S. Isaacson for his interest, patience and many helpful suggestions in the preparation of this paper. The author would also like to thank Michael Scheinfein and Andrew Muray for their support and friendship. Lastly, the author would like to thank Bonni Davis for typing the manuscript.

This work was supported by the NSF through grant No. ECS 8200312 to NRRFSS.

Appendix A

We first consider a variation of the Hankel–Schläfli contour integral [11], namely

$$\frac{1}{2\pi i} \int \frac{2(tJ_\nu(xw)J_{\nu+1}(tw) - xJ_\nu(tw)J_{\nu+1}(xw))}{(t^2 - x^2)J_\mu^2(w)} dw, \quad (\text{A.1})$$

where $x + t < 2$, ν is real, $\nu \geq -1/2$, and $\mu = \nu + p$ where p is an integer.

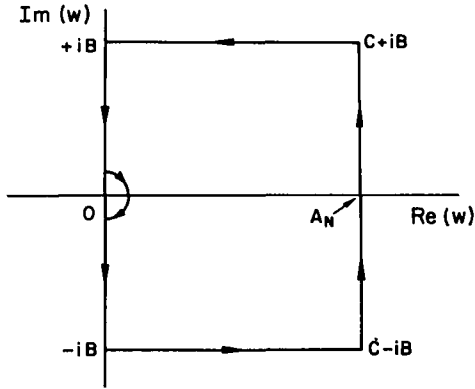


Fig. 12.

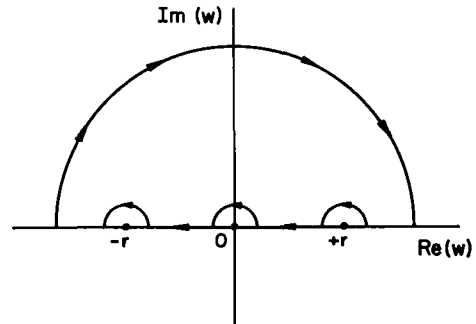


Fig. 13.

It can be verified that the residue of the integrand at $w = j_{\mu,m}$ is

$$2J_\nu(xj_{\mu,m})J_\nu(tj_{\mu,m})/J_{\mu\pm 1}^2(j_{\mu,m}), \tag{A.2}$$

where $j_{\mu,m}$ is the m th zero of $J_\mu(w)$ arranged in ascending order.

If $\mu \leq \nu$ then the residue at $w = 0$ is zero. If $\mu = \nu + 1$ then it can be verified that the residue at zero is

$$4(\nu + 1)x^\nu t^\nu. \tag{A.3}$$

We now consider the contour of integration as a partial rectangle with vertices $\pm Bi$, $C \pm Bi$, and with a side that crosses the real axis at A_N where A_N is chosen so that $j_N < A_N < j_{N+1}$. This is illustrated in fig. 12.

By considering the asymptotic value of the integrand for large argument, one finds that the integral along the upper and lower sides of the contour tend to zero as $B \rightarrow \infty$ provided that $x + t < 2$.

We can therefore write

$$\sum_{m=1}^N \frac{2J_\nu(xj_{\mu,m})J_\nu(tj_{\mu,m})}{J_{\mu+1}^2(j_{\mu,m})} = \frac{1}{2\pi i} \int_{c-i\infty}^{c+i\infty} g(w) dw + \frac{1}{2\pi i} \int_{-i\infty}^{+i\infty} g(w) dw, \tag{A.4}$$

where the contour for the integral on the right must cross the real axis at A_N , and where

$$g(w) = 2\{tJ_\nu(xw)J_{\nu+1}(tw) - xJ_\nu(tw)J_{\nu+1}(xw)\}/(t^2 - x^2)J_\mu^2(w). \tag{A.5}$$

Since $g(w)$ is an odd function of w , we not only notice that

$$C_0(t, x; \mu, \nu) \equiv \frac{1}{2\pi i} \int_{-i\infty}^{+i\infty} g(w) dw = \begin{cases} 0 & \text{if } \mu \leq \nu, \\ 2(\nu + 1)x^\nu t^\nu & \text{if } \mu = \nu + 1, \end{cases} \tag{A.6}$$

but we also notice that we can now write

$$T_N(t, x; \mu, \nu) = \frac{1}{2\pi i} \int_{A_N}^{c+i\infty} g(w) dw + \frac{1}{2\pi i} \int_{e^{i\pi}A_N}^{e^{i\pi}c+i\infty} g(w) dw. \tag{A.7}$$

where

$$T_N(t, x; \mu, \nu) = \sum_{m=1}^N \frac{2J_\nu(xj_{\mu,m})J_\nu(tj_{\mu,m})}{J_{\mu,m}^2(j_{\mu,m})} + C_0(t, x; \mu, \nu). \tag{A.8}$$

Now if we make the substitution

$$U(w) = w \{ tJ_\nu(xw)J_{\nu+1}(tw) - xJ_\nu(tw)J_{\nu+1}(xw) \} / (t^2 - x^2),$$

$$dV(w) = \frac{\pi}{i} \frac{J_\mu(w) \frac{\partial}{\partial w} [H_\mu^{(1)}(w)] - H_\mu^{(1)}(w) \frac{\partial}{\partial w} [J_\mu(w)]}{J_\mu^2(w)} dw = \frac{2dw}{wJ_\mu^2(w)},$$

where

$$dU(w) = wJ_\nu(xw)J_\nu(tw) dw, \quad V(w) = \frac{\pi}{i} \frac{H_\mu^{(1)}(w)}{J_\mu(w)}.$$

We can integrate eq. (A.7) by parts to obtain

$$T_N(t, x; \mu, \nu) = [U(e^{i\pi}A_N)V(e^{i\pi}A_N) - U(A_N)V(A_N)] \frac{1}{2\pi i} + \frac{1}{2\pi i} \int_{A_N}^{c+i\infty} V(w) dU(w)$$

$$+ \frac{1}{2\pi i} \int_{e^{i\pi}c+i\infty}^{e^{i\pi}A_N} V(w) dU(w).$$

Noting that $\mu = \nu + p$ where p is an integer and assuming ν is real, we can then write

$$T_N(t, x; \mu, \nu) = \frac{A_N \{ tJ_\nu(xA_N)J_{\nu+1}(tA_N) - xJ_\nu(tA_N)J_{\nu+1}(xA_N) \}}{t^2 - x^2}$$

$$- \frac{1}{2} \int_{A_N}^{c+i\infty} \frac{wJ_\nu(xw)J_\nu(tw)H_\mu^{(1)}(w)}{J_\mu(w)} dw$$

$$- \frac{1}{2} \int_{A_N}^{c+i\infty} \left(\frac{wJ_\nu(xw)J_\nu(tw)H_\mu^{(1)}(w)}{J_\mu(w)} dw \right)^*, \quad (\text{A.9})$$

where * denotes the complex conjugate[†]. If we now define $u \equiv xA_N$, $v \equiv tA_N$, we can make a change of variables and write

$$T_N(v/A_N, u/A_N; \mu, \nu)/A_N^2 = \frac{vJ_\nu(u)J_{\nu+1}(v) - uJ_\nu(v)J_{\nu+1}(u)}{v^2 - u^2}$$

$$- \int_1^{c+i\infty} \text{Re} \left\{ \frac{wJ_\nu(uw)J_\nu(vw)H_\mu^{(1)}(A_N w)}{J_\mu(A_N w)} dw \right\}. \quad (\text{A.10})$$

It is now illustrative to examine the asymptotic value of the above integral. If we set $w = \chi + iy$ then it can be shown that

$$\frac{H_\mu^{(1)}(A_N w)}{J_\mu(A_N w)} \approx 1 - \frac{\sinh(A_N y) \cosh(A_N y)}{\sinh^2(A_N y) + \cos^2(A_N \chi + \phi)} + i \frac{\sin(A_N \chi + \phi) \cos(A_N \chi + \phi)}{\sinh^2(A_N y) + \cos^2(A_N \chi + \phi)}, \quad (\text{A.11})$$

[†] This follows from the verifiable fact that

$$\frac{-w^* J_\nu(-xw^*) J_\nu(-tw^*) H_\mu^{(1)}(-w^*)}{J_\mu(-w^*)} = \left(\frac{wJ_\nu(xw)J_\nu(tw)H_\mu^{(1)}(w)}{J_\mu(w)} \right)^*$$

for real ν .

where $\phi = -\pi\mu/2 - \pi/4$. If we choose $\chi = 1$ and $A_N = j_{\mu,N}$ we can see that

$$H_\mu^{(1)}(j_N + i j_N y) / J_\mu(j_N + i j_N y) \approx -e^{-j_N y} / \sinh(j_N y). \quad (\text{A.12})$$

If we now take the dominant terms in the asymptotic expansion of $wJ_\nu(uw)J_\nu(vw)$ we obtain

$$-\int_1^{1+i\infty} \text{Re} \left\{ \frac{wJ_\nu(uw)J_\nu(vw)H_\mu^{(1)}(j_N w)}{J_\mu(j_N w)} dw \right\} \approx \frac{2}{\pi\sqrt{uv}} \int_0^\infty \frac{e^{-j_N y}}{\sinh(j_N y)} d(u, v, y) dy, \quad (\text{A.13})$$

where

$$d(u, v, y) = [\sinh(uy) \cosh(vy) \sin(u + \phi) \cos(v + \phi) + \sinh(vy) \cosh(uy) \sin(v + \phi) \cos(u + \phi)].$$

This integral can now be evaluated by taking y as a complex variable and integrating the integrand of (A.13) around the rectangular contour with vertices $0, \pi i/j_N, A, A + \pi i/j_N$. Taken in the limit $A \rightarrow \infty$, we obtain

$$\begin{aligned} \frac{2}{\pi\sqrt{uv}} \int_0^\infty \frac{e^{-j_N y}}{\sinh(j_N y)} d(u, v, y) dy &= \frac{2}{\pi\sqrt{uv}} \frac{u \sin(u + \phi) \cos(v + \phi) - v \sin(v + \phi) \cos(u + \phi)}{u^2 - v^2} \\ &- \frac{1}{j_N \sqrt{uv}} \frac{\sin \frac{\pi u}{j_N} \sin(u + \phi) \cos(v + \phi) - \sin \frac{\pi v}{j_N} \sin(v + \phi) \cos(u + \phi)}{\cos(\pi v/j_N) - \cos(\pi u/j_N)}. \end{aligned} \quad (\text{A.14})$$

We can now write

$$\begin{aligned} -\int_1^{c+i\infty} \text{Re} \left\{ \frac{wJ_\nu(uw)J_\nu(vw)H_\mu^{(1)}(j_N w)}{J_\mu(j_N w)} dw \right\} \\ \approx \frac{uJ_\nu(u)J_{\nu+1}(v) - vJ_\nu(v)J_{\nu+1}(u)}{v^2 - u^2} - \frac{\pi}{2j_N} \frac{\sin \frac{\pi u}{j_N} J_{\nu+1}(u)J_\nu(v) - \sin \frac{\pi v}{j_N} J_{\nu+1}(v)J_\nu(u)}{\cos(\pi v/j_N) - \cos(\pi u/j_N)}. \end{aligned} \quad (\text{A.15})$$

Thus we can write

$$T_N \left(\frac{v}{j_{\mu,N}}, \frac{u}{j_{\mu,N}}; \mu, \nu \right) \frac{1}{j_{\mu,N}^2} \approx \frac{\pi}{2j_{\mu,N}} \frac{\sin \frac{\pi u}{j_{\mu,N}} J_{\nu+1}(u)J_\nu(v) - \sin \frac{\pi v}{j_{\mu,N}} J_{\nu+1}(v)J_\nu(u)}{\cos(\pi u/j_{\mu,N}) - \cos(\pi v/j_{\mu,N})} \quad (\text{A.16})$$

for $u, v < j_{\mu,N}$.

We now can establish a few fundamental properties of the function

$$T_N \left(\frac{v}{j_{\mu,N}}, \frac{u}{j_{\mu,N}}; \mu, \nu \right) \frac{1}{j_{\mu,N}^2}.$$

From the asymptotic expansion of $H_\mu^{(1)}(j_N w) / J_\mu(j_N w)$ in eq. (A.12), it is clear that if we choose $u = j_p$ then

$$\lim_{N \rightarrow \infty} \frac{(j_N + i j_N \rho) J_\nu(j_p + i j_p \rho) J_\nu(v + i v \rho) H_\mu^{(1)}(j_N + i j_N \rho)}{J_\mu(j_N + i j_N \rho)} = \begin{cases} 0, & \rho > 0, \\ \text{bounded}, & \rho = 0, \end{cases}$$

Therefore it is apparent that the integral in the latter part of eq. (A.10) is zero in this limit. Thus, we may write

$$\lim_{N \rightarrow \infty} T_N \left(\frac{v}{j_{\mu,N}}, \frac{j_{\nu,p}}{j_{\mu,N}}; \mu, \nu \right) \frac{1}{j_{\mu,N}^2} = \frac{j_{\nu,p} J_{\nu+1}(j_{\mu,p}) J_{\nu}(v)}{j_{\nu,p}^2 - v^2} \quad (\text{A.18})$$

and for $v = j_{\nu,k}$

$$\lim_{N \rightarrow \infty} T_N \left(\frac{j_{\nu,k}}{j_{\mu,N}}, \frac{j_{\nu,p}}{j_{\mu,N}}; \mu, \nu \right) \frac{1}{j_{\mu,N}^2} = \frac{\delta_{p,k} J_{\nu+1}^2(j_{\mu,p})}{2}.$$

This is the desired orthogonality relation (eq. (11)) for the limiting case $N \rightarrow \infty$. For finite N , eq. (A.16) strongly suggests that

$$T_N \left(\frac{j_{\nu,k}}{j_{\mu,N}}, \frac{j_{\nu,p}}{j_{\mu,N}}; \mu, \nu \right) \frac{1}{j_{\mu,N}^2} = \frac{\delta_{p,k} J_{\nu+1}^2(j_{\mu,p})}{2}. \quad (\text{A.19})$$

When one numerically evaluates $T_N(j_{\nu,r}/j_{\mu,N}, j_{\nu,p}/j_{\mu,N}; \mu, \nu)$ one finds that relationship (A.19) is exact to within the limits of computational error ($\pm 10^{-7}$) for $\mu = \nu = 0$ and for zeros calculated accurately to 7 decimal places. If, however, the smallest value of N is taken ($N = 1$) we find

$$4J_0(j_1^2/j_2)/J_1^4(j_1)j_2^2 = 0.9999739.$$

The deviation from expression (A.19) for this case is 2.61×10^{-5} . If we take the appropriate Taylor expansions of the above expression, it is found that the expected computational error should be about 100 times less. Thus, it appears that the relationship may not be analytically exact.

For all other values of μ and ν it is found that for values of $N > 30$ that (A.19) holds to within the limits of computational error ($\pm 10^{-7}$). For smaller values of N , the relationship does not hold exactly. The worst case ($N = 1$) giving a deviation from eq. (A.19) of at most $\pm 10^{-3}$.

As a point of additional interest, if we now choose $\chi = 1$ and $A_N = K_{\mu,N} \equiv (j_{\mu,N} + j_{\mu,N+1})/2$ in eq. (A.11) to obtain

$$\frac{H_{\mu}^{(1)}(K_{\mu,N} + iK_{\mu,N}\mathcal{Y})}{J_{\mu}(K_{\mu,N} + iK_{\mu,N}\mathcal{Y})} \approx \frac{e^{-K_{\mu,N}\mathcal{Y}}}{\cosh(K_{\mu,N}\mathcal{Y})},$$

we can evaluate expression (A.9) in a similar manner as before to obtain

$$\begin{aligned} & T_N \left(\frac{v}{K_{\mu,N}}, \frac{u}{K_{\mu,N}}; \mu, \nu \right) \frac{1}{K_{\mu,N}^2} \\ & \approx \frac{\pi}{2K_{\mu,N}} \frac{\sin \frac{\pi u}{2K_{\mu,N}} \cos \frac{\pi v}{2K_{\mu,N}} J_{\nu+1}(u) J_{\nu}(v) - \sin \frac{\pi v}{2K_{\mu,N}} \cos \frac{\pi u}{2K_{\mu,N}} J_{\nu+1}(v) J_{\nu}(u)}{\cos(\pi u/K_{\mu,N}) - \cos(\pi v/K_{\mu,N})}. \end{aligned} \quad (\text{A.20})$$

This relationship yields a whole new set of orthogonality relations which include all those given in eqs. (11), (16)–(19) with j_N replaced by $\frac{1}{2}(j_N + j_{N+1})$.

Appendix B

Eqs. (16) and (17) follow immediately from eq. (A.16).

We can derive eq. (18) by writing eq. (10) as

$$f(j_k T / \lambda_N) = \sum_{m=1}^N \frac{2F_{\nu+1}(\lambda_m / T)}{J_{\nu}^2(\lambda_m) T^2} J_{\nu+1}(\lambda_m j_k / \lambda_N) \quad (\text{B.1})$$

if we now multiply both sides by $2J_{\nu}(\lambda_p j_k / \lambda_N) / J_{\nu+1}^2(j_k) \lambda_N^2$ and sum with respect to k , by utilizing relationship (17) we obtain

$$\sum_{k=1}^N \frac{T^2}{\lambda_N^2} \frac{2f(j_k T / \lambda_N)}{J_{\nu+1}^2(j_k)} J_{\nu+1}(j_k \lambda_p / \lambda_N) = \begin{cases} F_{\nu+1}(\lambda_p / T), & p < N, \\ \frac{4N}{J_{\nu}^2(\lambda_N) \lambda_N^2} F_{\nu+1}(T), & p = N. \end{cases} \quad (\text{B.2})$$

If we now multiply both sides of the above equation by $2J_{\nu+1}(\lambda_p j_m / \lambda_N) / J_{\nu}^2(\lambda_p) \lambda_N^2$ and sum p from 0 to N , we obtain (after a little algebra)

$$\begin{aligned} & \sum_{p=1}^N \frac{2F_{\nu+1}(\lambda_p T / \lambda_N)}{J_{\nu}^2(\lambda_p) T^2} J_{\nu+1}(\lambda_p j_k / \lambda_N) \\ &= \sum_{k=1}^N \left[\frac{2f(j_k T / \lambda_N)}{J_{\nu+1}^2(j_k)} \sum_{p=1}^{N-1} \frac{2J_{\nu+1}(\lambda_p j_k / \lambda_N) J_{\nu+1}(\lambda_p j_m / \lambda_N)}{J_{\nu}^2(\lambda_p) \lambda_N^2} + \frac{J_{\nu+1}(j_k) J_{\nu+1}(j_m)}{2N} \right]. \end{aligned} \quad (\text{B.3})$$

On comparison with eq. (B.1) we obtain

$$\sum_{p=1}^{N-1} \frac{2J_{\nu+1}(\lambda_p j_k / \lambda_N) J_{\nu+1}(\lambda_p j_m / \lambda_N)}{J_{\nu}^2(\lambda_p) \lambda_N^2} = \delta_{m,k} \frac{J_{\nu+1}^2(j_k)}{2} - \frac{J_{\nu+1}(j_k) J_{\nu+1}(j_m)}{2N} + \epsilon.$$

Appendix C

Eq. (19) can be derived using a similar contour integral to that used in appendix A, such as integrating

$$\frac{1}{2\pi i} \int \frac{J_{\nu+1}(\lambda_k w / j_N) \{ J_{\nu}(w) H_{\nu}^{(1)}(j_k w / j_N) - J_{\nu}(j_k w / j_N) H_{\nu}^{(1)}(w) \}}{J_{\nu}(w)} dw$$

over the same contour illustrated in fig. 12. We can also, however, integrate a variation on Hankel's integral [11] namely

$$\frac{1}{2\pi i} \int \frac{J_{\nu+1}(az) H_{\nu}^{(1)}(bz)}{z^2 - r^2} dz$$

over the contour as illustrated in fig. 13, where B is allowed to approach infinitely and where the indentations about the origin and around the singularities at $\pm r$ are allowed to become infinitely small. Taking the real part of this result, we obtain

$$\int_0^{\infty} \frac{J_{\nu}(bz) J_{\nu+1}(az)}{z^2 - w^2} dz = \frac{\pi i}{2} \frac{J_{\nu+1}(aw) N_{\nu}(bw)}{w}, \quad b > a, \quad (\text{C.1})$$

letting $b = j_N$, $w = j_p/j_N$, $a = \alpha j_N$ and $\alpha < 1$, we see

$$\int_0^\infty \frac{J_\nu(j_N z) J_{\nu+1}(\alpha z j_N) dz}{j_p^2 - z^2 j_N^2} = \frac{J_{\nu+1}(\alpha j_p)}{j_p^2 J_{\nu+1}(j_p) j_N}, \quad \alpha < 1. \quad (\text{C.2})$$

Utilizing this result to integrate eq. (9) directly we obtain

$$\int_0^\infty F_\nu(r j_N/T) J_{\nu+1}(\alpha r j_N) dr = \sum_{m=1}^{N-1} \frac{2 F_\nu(j_m/T) J_{\nu+1}(\alpha j_m)}{J_{\nu+1}^2(j_m) j_m j_N}, \quad (\text{C.3})$$

if we now use algorithm (13) we obtain

$$\int_0^\infty F_\nu(r j_N/T) J_{\nu+1}(\alpha r j_N) dr = \sum_{p=1}^{N-1} \frac{2 f(j_p T/j_N)}{J_{\nu+1}^2(j_p)} \sum_{m=1}^{N-1} \frac{2 J_\nu(j_p j_m/j_N) J_{\nu+1}(\alpha j_m)}{J_{\nu+1}^2(j_m) j_m j_N} \frac{T^2}{j_N^2}.$$

According to eq. (14), we can write the left-hand side of the above equation as

$$\begin{aligned} & \frac{T^2}{j_N^2} \sum_{p=1}^{N-1} \frac{2 f(j_p T/j_N)}{J_{\nu+1}^2(j_p)} \int_0^1 J_\nu(j_p r) J_{\nu+1}(\alpha r j_N) dr \\ & \approx \frac{T^2}{j_N^2} \sum_{p=1}^{N-1} \frac{2 f(j_p T/j_N)}{J_{\nu+1}^2(j_p)} \sum_{m=1}^{N-1} \frac{2 J_\nu(j_p j_m/j_N) J_{\nu+1}(\alpha j_m)}{J_{\nu+1}^2(j_m) j_m j_N} \end{aligned} \quad (\text{C.4})$$

which yields the desired result

$$\int_0^1 J_\nu(j_p r) J_{\nu+1}(\alpha r j_N) dr \approx \sum_{m=1}^{N-1} \frac{2 J_\nu(j_p j_m/j_N) J_{\nu+1}(\alpha j_m)}{J_{\nu+1}^2(j_m) j_m j_N}. \quad (\text{C.5})$$

References

- [1] J. Brunol and P. Chavel, IEEE Proc. 65 (1978) 1089.
- [2] S.M. Candel, Comput. Phys. Commun. 23 (1981) 343.
- [3] A.V. Oppenheim et al., IEEE Proc. 66 (1978) 264.
- [4] A.V. Chave, Geophys. 48 (1983) 1671.
- [5] A. Siegman, Opt. Lett. 1 (1977) 13.
- [6] D.R. Moor, IEEE Trans. on Acoustics, Speech and Signal Processing ASSP-31 (1983) 979.
- [7] W.L. Anderson, Geophys. 44 (1979) 1287.
- [8] P.K. Murphy and N.C. Gallagher, J. Opt. Soc. Am. 73 (1983) 1130.
- [9] I.M. Sneddon, Fourier Transforms (McGraw-Hill, New York, 1951).
- [10] P.E. Batson, Ph.D. Thesis, Cornell University (1976).
- [11] G.N. Watson, Theory of Bessel Functions (Cambridge, Univ. Press. London, 1922).
- [12] F. Lenz, Z. Naturforsch. A9 (1954) 185.
- [13] A.V. Crewe and T. Groves, J. Appl. Phys. 45 (1974) 3662.